Geophys. J. Int. (2003) **155,** 839–856

Lateral variations of seismic intensity attenuation in Italy

Francescantonia Carletti and Paolo Gasperini

Dipartimento di Fisica, Alma Mater Studiorum, Università di Bologna, Italy. E-mail: paolo@ibogfs.df.unibo.it

Accepted 2003 July 1. Received 2003 June 26; in original form 2002 May 23

SUMMARY

A tomographic study of the attenuation of seismic intensity in the Italian territory has been carried on the basis of a felt report database including more than 50 000 macroseismic observations. The spatial variations of the attenuation coefficients have been computed on meshes of 50 and 25 km and compared with other geophysical observables. By checkerboard and restore tests using a Gaussian error with a realistic amplitude of one intensity degree we verified that a selected set including about 20 000 observations is able to reliably reproduce the imposed patterns. For the laterally varying attenuation model we also found a general reduction and a more uniform distribution of the average locality residual with respect to an isotropic attenuation law. The comparison of the inversion results with seismic velocity tomography of the crust and upper mantle shows fair correspondences between high-attenuation and low-velocity areas (Tyrrhenian slope of northern and central Apennines) as well as between low-attenuation and high-velocity ones (Po valley and Adriatic coast). The normalized attenuation functions computed for some areas of Italy also agree fairly well with empirical non-parametric attenuation functions determined by others, from accelerometer data. A clear correlation was found between the inferred behaviour of the slope of the attenuation function in the vicinity of the source (distance <45 km) and the heat flow. In fact, the most attenuating zones almost coincide with the highs of heat flow located along the northern Tyrrhenian coast of Tuscany and Latium and in the other volcanic areas (Campi Flegrei, Mount Etna, Colli Euganei and Monti Lessini). This clear correlation represents a convincing confirmation of the physical grounds on which the use and interpretation of macroseismic data is based.

Key words: attenuation, macroseismic intensity, tomography.

INTRODUCTION

The use of seismic intensity to investigate the characteristics of seismic wave generation and propagation was almost discontinued in Italy and in most highly developed countries about 25 years ago. At that time the rapid improvement of modern seismometric and accelerometric networks made these basically qualitative data appear to most as outdated with respect to more accurate instrumental measurements. In some countries (including Italy) the analysis of macroseismic data was not dismissed albeit confined to the ambit of historical seismicity studies devoted to the compilation of seismic catalogues used in probabilistic seismic hazard assessment (PSHA). Over the last few years we have assisted instead in a revival of interest in such studies due to the increasing relevance of local characteristics of seismic waves propagation in seismic hazard assessment and even to the relatively poor efficiency of engineering methods to predict real damage from ground motion amplitudes.

Although the quality of the information given by a single intensity observation is certainly poorer with respect to the complete instrumental recordings of the ground motion, the wide availability of intensity data for almost every settlement struck by an earthquake makes them very useful for describing the local variations of seismic wave propagation properties. This is particularly true in the near field (less than 50–100 km from the source) where the instrumental data are sparse and sometimes not available at all. Moreover, the direct estimation of the expected intensity at a given site allows one to infer straightforwardly the amount of expected damage and casualties that could be induced by future earthquakes.

Differently from other seismic countries, in Italy PSHA are commonly computed not only in terms of Peak Ground Acceleration (PGA) but also in terms of seismic intensity (Slejko 1996; Romeo & Pugliese 1997). This is because most of the information available on past earthquakes (even for most of the 20th century) has been given in terms of seismic intensity rather than any other instrumental parameter. In fact, in Italy the availability of instrumental data is poor up to about 15 years ago when a digital seismic acquisition system has been installed at the Istituto Nazionale di Geofisica (ING) of Rome. On the other hand, the long cultural heritage of our country has allowed the preservation of a very large amount of information, in the form of chronicles or scholarly treaties, even regarding earthquakes that occurred several centuries ago. Therefore, the historical catalogue of Italian earthquakes can be considered almost complete

for earthquakes with magnitude larger than 5.5–6.0 starting from the 17th century (Gasperini & Ferrari 2000).

These high-quality macroseismic data have already been used by Gasperini *et al.* (1999) to reliably constrain the location, the orientation and the spatial dimension of the seismogenic faults for the largest earthquakes that occurred in central and southern Italy during the last four centuries. Furthermore, in a recent work, Gasperini (2001) used these data to make inferences on the physics of the attenuation of seismic energy in the vicinity of the source (less than 180 km). He found that the attenuation of the seismic intensity fits well a bilinear function characterized by two almost constant slopes of about one intensity degree per 20 km up to 45 km from the source and of about one intensity degree per 50 km at greater distances.

INTENSITY ATTENUATION MODELS

Since the first attempts by Kövesligethy (1906), previous analyses on the modelling of the seismic intensity attenuation with distance were guided by the empirical evidence that the difference between epicentral and local intensity increases monotonically with increasing distance, while its derivative decreases. Thus, in general the functional relation was chosen empirically among the class of continuous functions having a positive first derivative and a negative second derivative. Among others Berardi *et al.* (1993) proposed for Italy a cube-root attenuation model (CRAM) which, using only two free parameters, was shown to reproduce the behaviour of intensity data with distance better than almost any other similar model. However, Gasperini (2001) demonstrated that such a preference disappears if the incomplete classes of intensity data below the limit of diffuse perceptibility (about degree IV) are removed. In this case, other empirical functions (square or fourth root) might fit the data as well or even better.

Gupta & Nuttli (1976) proposed a more physically consistent approach to this problem. Assuming the intensity to be linearly related to the logarithm of the ratio between the amplitude and the period of seismic waves (A/T) they derived the equation

$$\Delta I = C_1 + C_2(k\Delta \log_{10} e + \log_{10} \Delta), \tag{1}$$

where Δ is the distance in degrees and k (γ in the original paper) is the coefficient of anelastic attenuation, while C_1 and C_2 are empirical constants. In this formula the linear term accounts for the anelastic dissipation while the logarithmic term accounts for the geometrical spreading. However, the analysis of variance (ANOVA) statistical test performed by Gasperini (2001) demonstrated that, in Italy, a bilinear model fits the data significantly better than the model of Gupta & Nuttli (1976) and any other reasonable simple model. The functional relation proposed by Gasperini (2001) is the following:

$$\Delta I = \begin{cases} \alpha + \beta D & (D \le 45) \\ \alpha + \beta 45 + \gamma(D - 45) & (D > 45), \end{cases} \tag{2}$$

where D is the hypocentral distance in kilometres, ΔI is the intensity difference, and α, β and γ are free parameters showing significant variations in different areas. The location of the slope change point at 45 km from the source was empirically estimated from the data and was found to be rather stable all over the Italian territory.

In view of the physical description given by Gupta & Nuttli (1976) the linear behaviour of the attenuation function could mean that anelastic dissipation is the prevailing attenuation mechanism in the Italian crust even at a relatively short distance from the epicentre. Moreover, the linear shape and the marked reduction of the slope in the second part of the curve would indicate a definitely less attenuating path (maybe deeper) for waves controlling intensity at distances larger than 45 km. A similar slope decrease at about 50 km from the source was already observed for PGA, in the case of the Loma Prieta earthquake (Somerville & Yoshimura 1990; Fletcher & Boatwright 1991; McGarr*et al.* 1991). Moreover, this behaviour was also predicted by numerical simulation of the attenuation of PGA and Arias intensity in central Italy (Fäh & Panza 1994). Gasperini (2001) also observed a correspondence of the regional variations of the far-field slope ($D > 45$ km) with refracted waves attenuation properties in Italy (Mele *et al.* 1996), which could indicate a subcrustal path of the phases controlling the radiation of seismic energy at such distances.

In spite of its statistical significance this simple bilinear model might appear to be not physically grounded due to the absence of a logarithmic term accounting for geometrical spreading. However, this apparent inconsistency between theory and observation could be explained by the combined effect of particularly high anelastic dissipation and a reduced 'effective' spreading exponent. We must note in fact, that Q values in the range 100–150 are typical of the central Apennines (Castro *et al.* 1999; Malagnini *et al.* 2000). These are not very different from rough estimates ($Q \approx 50$ for $\beta = 0.047$ and $Q \approx 150$ for $\gamma = 0.022$) that can be made from isotropic attenuation coefficients computed by Gasperini (2001). On the other hand, even at short hypocentral distances, the significant role played by surface and reflected phases (Somerville & Yoshimura 1990) and the effect of source dimensions can induce an apparent geometrical spreading exponent smaller than the theoretical value of -1 that was found to fit data well in many areas. Actually a spreading exponents ranging from 0 to -0.5 have been proposed to explain the decay of seismic waves in central Italy at distances larger than 30 km (Malagnini *et al.* 2000).

Certainly for small earthquakes and at very short distances (<10–20 km) the geometrical spreading dominates over dissipation but this is outside the observational window of the intensity data set. It could be hypothesized that the additional spreading decay, not properly modelled by the linear behaviour, is accounted for by the intercept term α of the bilinear law. All of these factors may well explain why the logarithmic behaviour, due to geometrical spreading, apparently disappears from Italian intensity attenuation curves even at relatively short distances.

Although this bilinear model needs to be confirmed by further studies, maybe using instrumental observations, it anyhow represents a statistically tested and physically meaningful starting point for analysing the lateral variation of attenuation characteristics in the Italian area. We thus assumed this general model for our analysis devoted to the mapping of the spatial variations of macroseismic intensity attenuation characteristics over the Italian territory.

In general, our analysis will consider the behaviour of 'total' attenuation, including spreading and anelastic dissipation as well as all other mechanisms that can induce a decrease of ground motion amplitude with distance. Our approach is to some degree different from previous macroseismic tomography analyses carried out in other areas (Hashida & Shimazaki 1984; Hashida *et al.* 1988; Papazachos 1992; Papazachos & Papaioannou 1997) as it does not assume *a priori* any functional relation between intensity and ground motion instrumental parameters.

DATA ANALYSIS

The data set analysed in the present work is exactly the same as that used by Gasperini (2001). It includes MCS intensity (Sieberg 1932)

data coming from two databases recently made available to the scientific community, which are the 'Catalogo dei Forti Terremoti in Italia dal 461 a. C. al 1990' (CFTI) (Boschi *et al.* 1997) and the 'Database delle Osservazioni Macrosismiche' (DOM) (Monachesi & Stucchi 1997). For the earthquakes (about 300) that are available from both of them, we followed the choices made in the 'consensus' joint catalogue (CPTI Working Group 1999), which was edited by the authors of the above two databases. The data set resulting from the application of these choices includes more than 50 000 MCS intensity observations, regarding about 1000 Italian earthquakes from ancient times until the present. To ensure the homogeneity of the determination of the intensities and of the derived source parameters, only the data coming from earthquakes occurring over the last two centuries (from 1801 until 1990), including intensity estimates in at least 20 different localities are used by Gasperini (2001) and in the present work. The macroseismic epicentre and the epicentral intensity of each earthquake are computed according to Gasperini & Ferrari (2000).

For every observation in the final intensity database (in total about 35 000), the hypocentre-to-locality path and the difference ΔI between the epicentre and the local intensity are considered. As for the majority of earthquakes included in our database, many of which belong to the pre-instrumental era, the centroid depth is not known; we assumed for all of them a fixed depth of 10 km. This is arbitrarily adopted here as being a representative value for a region such as Italy where significant earthquakes ($M > 5.0$), excluding a few intermediate events in the southern Tyrrhenian Sea (not included in our database), are relatively shallow ($h < 25$ km). Furthermore, just as for many international agencies, it is common practice for Italian seismological observatories (e.g. INGV) to fix a depth to 10 km when it cannot be otherwise computed from data. To reduce the path distortion in the vicinity of the source we excluded from our computations all macroseismic observations at sites located at an epicentral distance shorter than half of the subsurface rupture length (RLD), computed from the macroseismic magnitude by the Wells & Coppersmith (1994) formulae for 'all types of sources'. Moreover, to limit the bias due to incomplete reporting of low intensities (i.e. Gasperini 2001) we also excluded from the computations the data located at distances where the intensity predicted by the isotropic attenuation model was less than degree IV. In practice, this selection limits, as a function of the epicentral intensity, the maximum observable hypocentral distance, which for the largest earthquakes is about 180 km.

The distribution of hypocentre–site paths resulting from this data set (including about 20 000 observations) ensures fairly good coverage of most of the Italian continental territory (Fig. 1). In particular, the paths are quite dense along the Apennines Chain, in eastern Sicily and in the southeastern Alps, while they are rather sparse in the Central Alps, along the Tyrrhenian coast of Tuscany, in Apulia and in southeastern Sicily (see Fig. 2 for the location of the Italian region and structures). They are obviously almost absent over the seas and also in the islands of Corsica and Sardinia, as these areas are almost aseismic.

We performed our 2-D tomographic inversion over a grid of square cells covering the whole area represented in Fig. 1. The choice of the size of the cells is a critical point as a finer grid gives better resolution, while a coarser one grants a higher reliability to the inversion. On the basis of a comparison among the results of preliminary inversions made with grid sizes ranging from 25 to 200 km, we chose 50 km as the best compromise between resolution and reliability for the whole Italian territory. However, we found that even a grid size of 25 km can be appropriate in areas that are particularly well covered by source–receiver (hypocentre–locality) paths.

For any given intensity data in our database we can build an observation equation accounting for the contribution to intensity attenuation of each cell crossed by the hypocentre–locality path. As hypocentral distances are mostly shorter than 200 km we can work in the plane geometry neglecting the sphericity of the Earth. To minimize the effects of this approximation we converted the geographical coordinates of epicentres and localities to Cartesian kilometric coordinates by a Lambert conformal transformation. We also assumed the straightness of paths when computing their intersections with cell boundaries and the corresponding distances from the epicentres. For the sample case shown in Fig. 3 the resulting attenuation equation can be written as

$$\Delta I = \alpha + \beta_3 D_1 + \beta_{13}(D_2 - D_1) + \beta_{14}(45 - D_2) + \gamma_{14}(D_3 - 45) + \gamma_{24}(D_4 - D_3) + \gamma_{25}(D_5 - D_4) + \gamma_{35}(D - D_5), \quad (3)$$

where $\Delta I = I_0 - I$ is the epicentral-to-local intensity difference, D_l are the hypocentral distances of the intersections of the path with the cell boundaries and α, β_k and γ_k are the unknown attenuation parameters. As the true path followed by seismic phases (direct, refracted or reflected) inducing most significant effects on building and humans is not known exactly, we assumed a simple rectilinear inclined path from the source (at 10 km depth for all earthquakes) to the observing site on the Earth's surface (Fig. 3). This is a rather rough approximation that, however, is reasonably appropriate in the vicinity of the source where the effects of depth are more relevant. We stress again that the inclusion of depth in the attenuation equation is intended to correct, partially, for the bias induced at very short distances (<20–30 km) and not to reproduce a realistic wave path. It does not imply or require the assumption of a specific path for waves producing the most significant macroseismic effects. A geophysical interpretation, in terms of spatial and depth variations of seismic wave speeds and attenuation, may remain ambiguous, and the correlations with other physical properties are necessary but not sufficient evidence for a correct interpretation. Nevertheless, as shown below, this simple ray geometry is successful in producing a good statistical description of attenuation characteristics, as needed for hazard assessment, as the principal result of this paper.

Following Gasperini (2001), the parameter α of the bilinear law should account for discrepancy between computed and observed I_0 and for other local effects. We already noted above how α might also reflect the extra attenuation, due to the geometrical spreading, not accounted for by the other two coefficients. However, its separate estimation, for each earthquake or for each cell, is likely to be biased by the near-field attenuation properties of the cell (parameter β). A strong correlation between α and β had actually been observed in earlier computations where α was allowed to vary in each cell including at least one earthquake. For this reasons in the present formulation of the tomographic problem we considered a single common value of this parameter for all of the cells.

The application of this procedure to all of the N hypocentre–locality paths of our database gives the system of observation equations defining the tomographic problem. P is the total number of cells, α, β_p and γ_p (with $p = 1, \ldots, P$) form the unknown parameters vector m_l (with $l = 1, \ldots, 2P + 1$), while the known terms vector b_n (with $n = 1, \ldots, N$) is composed of the values of the intensity difference ΔI and the matrix of the unknown coefficients c_{nl} by the distance differences of eq. (1).

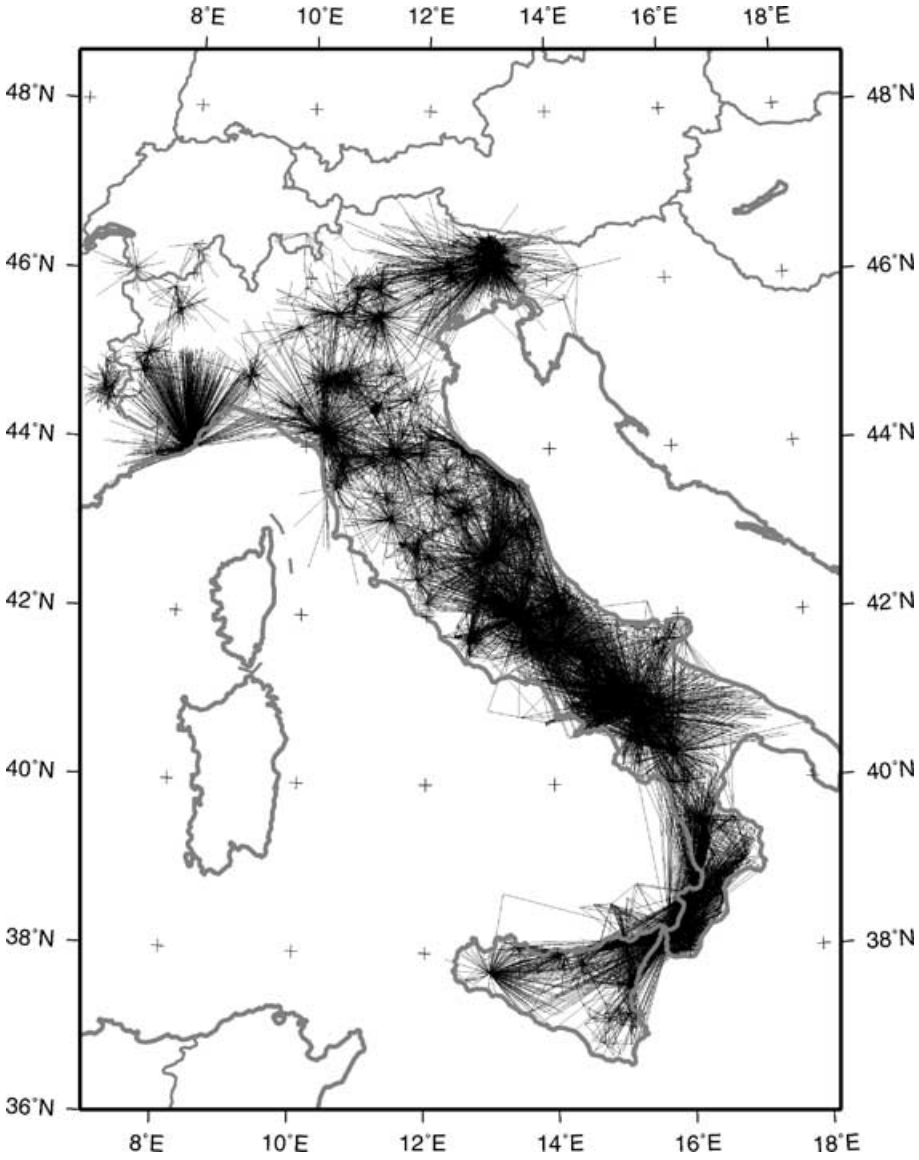

Figure 1. Epicentre to locality paths (about 20 000) used for the tomographic inversion of the seismic intensity attenuation coefficient in Italy.

As these equations are linear in nature they could be straightforwardly used to build the least-squares equation

$$g_{ij} \cdot m_j = d_i, \tag{4}$$

where $g_{ij} = c_{ki}c_{kj}$ and $d_i = c_{ni}b_n$.

However, to make the problem more similar to classical seismic wave tomography we redefine the system of equations in a differential form using as reference the values of the attenuation parameters α, β and γ computed for an isotropic model. The values of these parameters we computed for our data set are $\alpha = 0.445$, $\beta = 0.059$ and $\gamma = 0.0207$. The rms of such an inversion is 1.04 intensity degrees and the coefficient of variation is $R^2 = 0.56$. The parameter values slightly deviate from those computed by Gasperini (2001), as in that work the details of the least-squares fit were different with respect to the present one. In this study, in fact, we considered all the macroseismic observations as independent data without grouping them over distance bins as done by Gasperini (2001). However, it easy to verify that the maximum differences between the two attenuation curves remain smaller than one-tenth of an intensity degree over the whole range of distances from 0 to 180 km, and hence the two curves can be considered as coincident in practice. For the same sample case shown above, the observation equation in differential form becomes

$$\begin{aligned}\Delta I_{\rm obs} - \Delta I_{\rm exp} = I_{\rm exp} - I_{\rm obs} &= \Delta\beta_3 D_1 + \Delta\beta_{13}(D_2 - D_1) \\ &+ \Delta\beta_{14}(45 - D_2) + \Delta\gamma_{14}(D_3 - 45) \\ &+ \Delta\gamma_{24}(D_4 - D_3) + \Delta\gamma_{25}(D_5 - D_4) \\ &+ \Delta\gamma_{35}(D - D_5).\end{aligned} \tag{5}$$

In eq. (4) the unknowns vector m_j is now composed by the deviations $\Delta\beta_p$ and $\Delta\gamma_p$ of the attenuation coefficients in each cell from the reference isotropic values and the known terms vector by the differences between the observed intensity decrement $\Delta I_{\rm obs}$ and the intensity decrement $\Delta I_{\rm exp}$, which is expected on the basis of the isotropic attenuation equation.

To solve the least-squares system of equations we used the QR factoring least-squares method that could be shown to give a better computational efficiency and a higher quality solution with respect to the other inversion techniques with which we have experimented. This algorithm (implemented by the DLSQRR routine of the

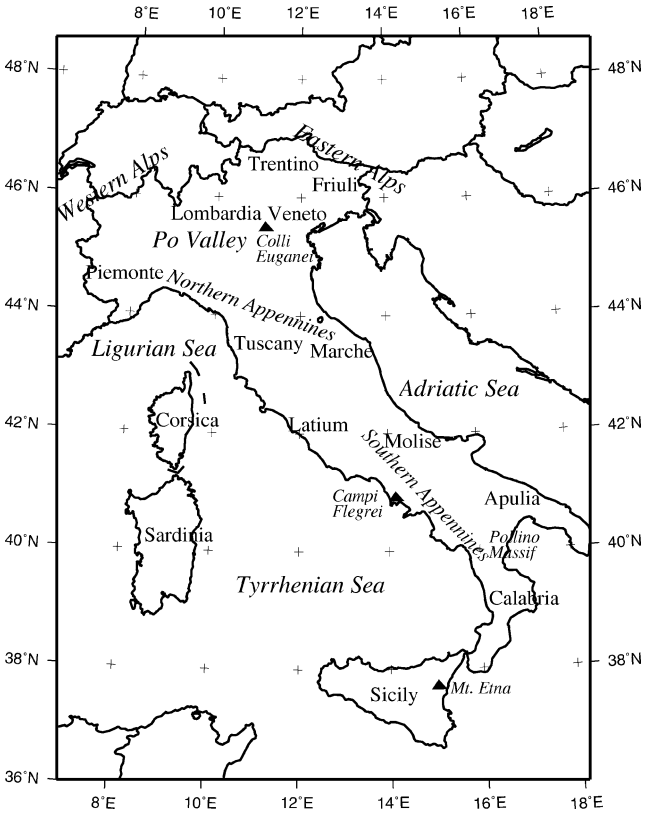

Figure 2. Map of Italy with the location of areas and structures mentioned in the text.

standard IMSL library of Compaq Visual Fortran 6.0) does not include damping but simply excludes from the inversion the unknowns that are poorly or not constrained at all by the data. This is a very common case in our problem as the macroseismic paths mainly cross the cells located in the continental part of Italy (about one quarter of the total cells in the area of Fig. 1).

CHECKERBOARD TESTING

In order to evaluate the ability of our data set to reliably constrain the tomographic inversion, we performed a checkerboard test using the path distribution of our real data set. We simulated a harmonic periodic pattern with a wavelength of 200 km (four 50 km cells) both in latitude and in longitude for both parameters β and γ. Figs 4(a) and 3(b) show the result of the inversion for parameters β and γ, respectively, when no noise is added to the theoretical intensity difference. We can see how the input patterns, with amplitudes of 0.045 and 0.015 for β and γ, respectively, are almost perfectly reproduced even in the cells crossed by very few paths. We can also note how the solution algorithm correctly excludes from the inversion the cells not crossed by any path. The inverted cells are 160 for coefficient β and 184 for coefficient γ.

To evaluate the goodness of the fit between the input and the computed values we defined three misfit estimators corresponding to the standard deviations between input and inverted values, normalized with respect to the input ranges of variation. They give an estimate of the relative uncertainties induced by random intensity errors on the estimated parameter values. The first two (M_β and M_γ) concern the two coefficients separately, while the third (M_T) is the sum of the two:

$$M_\beta = \sqrt{\frac{\sum_{j=1}^{n_\beta}\left(\beta_j^{\mathrm{i}} - \beta_j^{\mathrm{c}}\right)^2}{(0.045)^2 n_\beta}}$$

$$M_\gamma = \sqrt{\frac{\sum_{j=1}^{n_\gamma}\left(\gamma_j^{\mathrm{i}} - \gamma_j^{\mathrm{c}}\right)^2}{(0.015)^2 n_\gamma}}$$

$$M_T = \sqrt{\frac{\left[\sum_{j=1}^{n_\beta}\left(\beta_j^{\mathrm{i}} - \beta_j^{\mathrm{c}}\right)^2\right]/(0.045)^2 + \left[\sum_{j=1}^{n_\gamma}\left(\gamma_j^{\mathrm{i}} - \gamma_j^{\mathrm{c}}\right)^2\right]/(0.015)^2}{n_\beta + n_\gamma}}, \quad (6)$$

where β_j^{i}, β_j^{c}, γ_j^{i} and γ_j^{c} are the input and computed values of the attenuation coefficients in the jth inverted cells, and n_β and n_γ are the total number of inverted cells for coefficients β and γ, respectively. The values of such misfit estimators for the error-free inversion of Figs 4(a) and (c) are almost zero.

In Figs 4(c) and (d) we simulated instead a more realistic case by adding, to the theoretical intensity difference, a Gaussian random noise with amplitude of one intensity degree, corresponding to the standard deviation of real intensity data with respect to the isotropic model. In order to reproduce the true experimental framework realistically, we also rounded the simulated intensities to the nearest half-integer value. The accuracy of the inversion now appears rather variable and really poor for the cells crossed by a small number of paths. This can be better understood by examining, in Figs 5(a) and (b), the paths densities reported as the decimal logarithm of the number of paths crossings each cell for β and γ coefficients, respectively. From the comparison with Figs 4(c) and (d) we can verify how the inversion is not accurate for cells crossed by fewer than a few tens of paths. In poorly resolved cells (mainly located at the boundaries of the resolved domain), the inverted parameters sometimes assume values well outside of a reasonable range (white and black shades in Figs 4c and d). In particular, some negative deviations clearly exceed the central reference values for both β and γ, thus implying a negative slope for the attenuation function in such cells (the intensity increasing with distance), which can hardly be physically justified. This situation produces very high values for the misfits ($M_\beta = 11$, $M_\gamma = 32$ and $M_T = 25$), which indicates the inadequacy of the formulation in this case.

As the badly resolved cells can contaminate the results of the whole inversion we decided to redo the same computations but limiting the analysis to the cells crossed by at least 30 paths. This reduces the number of inverted cells to 111 and 100 for β and γ, respectively, but now the computed pattern of coefficient β (Fig. 5c) appears almost perfectly reproducing the imposed one over the entire considered area, while for γ the pattern (Fig. 5d) is quite well reproduced for central and southern Italy and only in the northern area are some significant discrepancies present. In this case the values of misfits ($M_\beta = 0.22$, $M_\gamma = 0.41$ and $M_T = 0.32$) tell us that the random errors on intensity affect the estimated values of β of about 20 per cent and for γ of about 40 per cent of the input amplitude of variation. On the basis of such evidence we can accept the inversion results for coefficient β, as well as to a lesser extent for coefficient γ, as reliable.

RESULTS OF REAL DATA INVERSION

Figs 6 and 7 show the results of the inversion of real data for parameters β and γ, respectively. The rms of such an inversion is 0.91 while the coefficient of variation is $R^2 = 0.64$, corresponding to a variance reduction of about 14 per cent with respect to the isotropic model. We tested the statistical significance of this better fit by the ANOVA test applied to the extra sum of squares (Draper & Smith

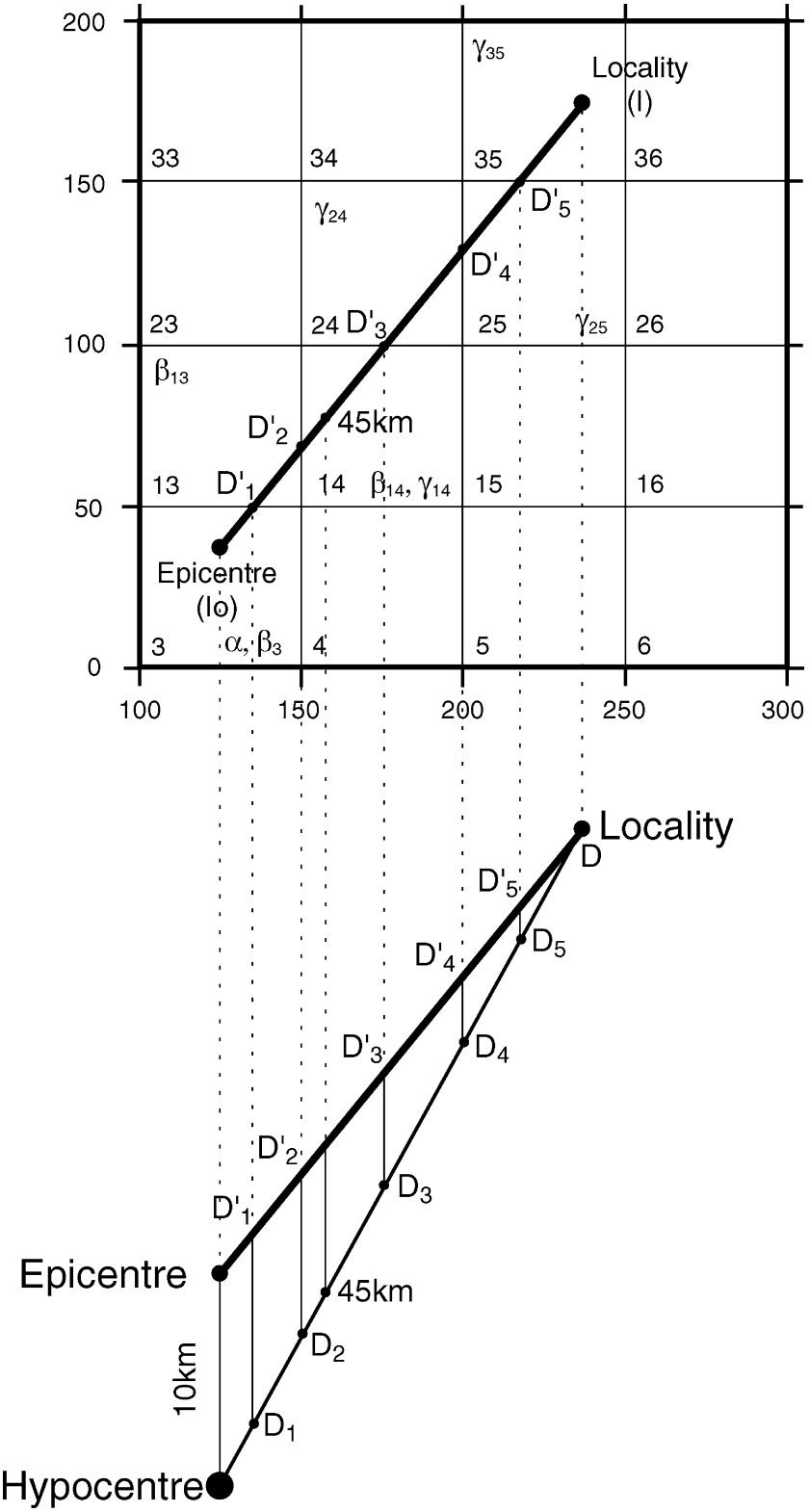

Figure 3. Geometrical sketch of the hypocentre–locality path decomposition used to compute the contribution of each cell to the attenuation equation.

1981, pp. 97–98) resulting from the application of the tomographic model with respect to the simpler isotropic one. The value of the F statistics for added terms $F = 16.1$ (with 209 numerator and 19 774 denominator degrees of freedom) indicates that in spite of the increase from three to 211 free parameters, the variance reduction is statistically significant with significance level s.l. < 0.01. We also evaluated the spatial correlation between the attenuation coefficients β and γ, computing a linear regression between the values of the two coefficients in the same cells. The values of the slope $b = -0.09 \pm 0.06$, of the intercept $a = 0.0016 \pm 0.0014$ and

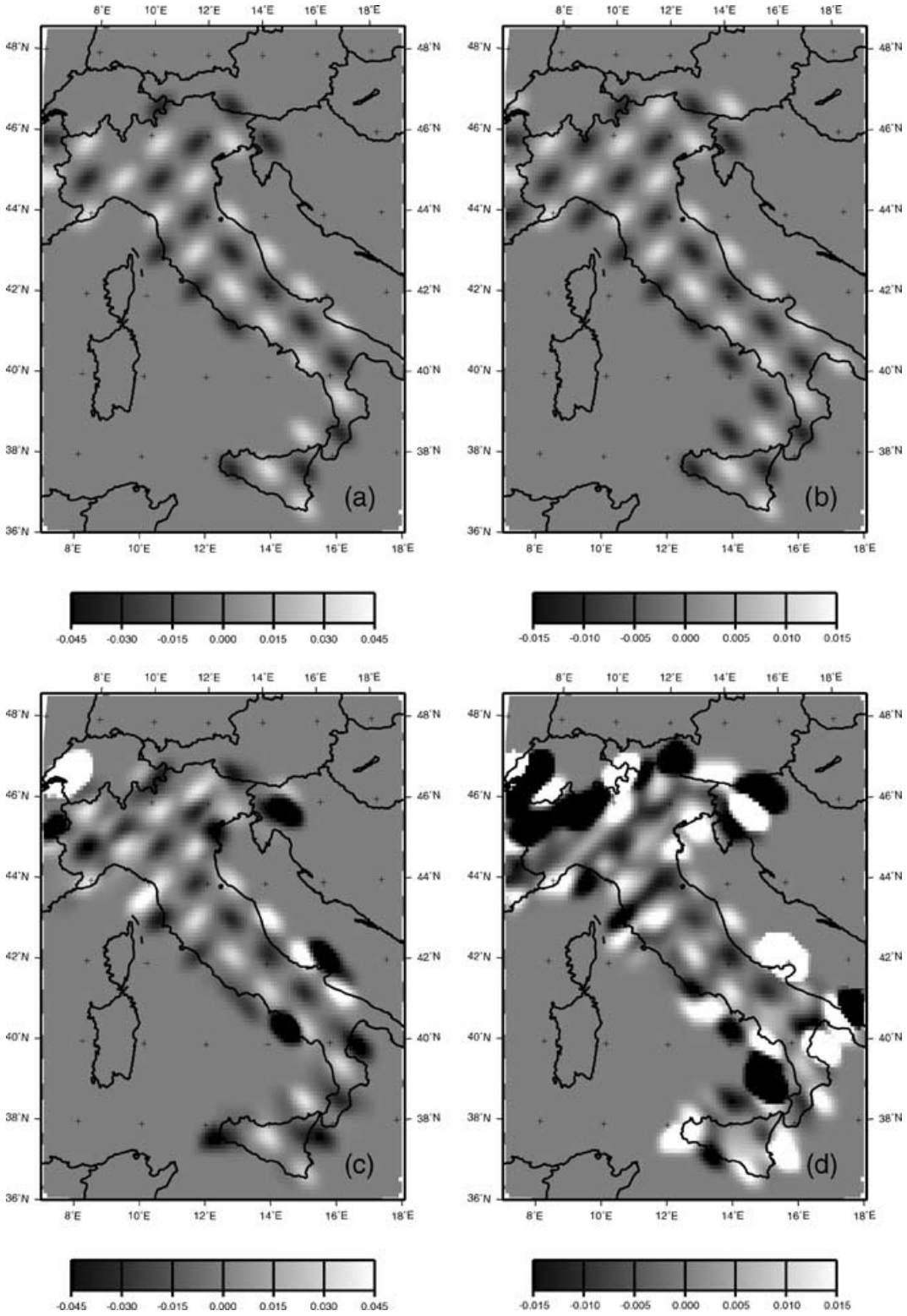

Figure 4. Results of the inversion over a 50 km mesh of a checkerboard harmonic pattern imposed on the attenuation coefficients β and γ, with a wavelength of 200 km, without (a), (b) and with (c), (d) Gaussian noise added and half-integer rounding of simulated intensities. Black and white shades correspond to values outside the imposed variation range.

of the coefficient of variation $R^2 = 0.01$ clearly indicate that no significant spatial correlation exists among the near-field and far-field attenuation coefficients.

Regarding the slope β of the first trait of the attenuation curve ($D \leq 45$ km), we can see (Fig. 6) how the zones with high attenuation are concentrated mainly in the Tyrrhenian slope of the northern and central Apennines and in the proximity of active volcanic areas (Campi Flegrei and Mt Etna). The attenuation is also relatively high in the Veneto-Friuli area (northeast of Italy), along the Adriatic coast of Molise (around latitude 42°) and in western

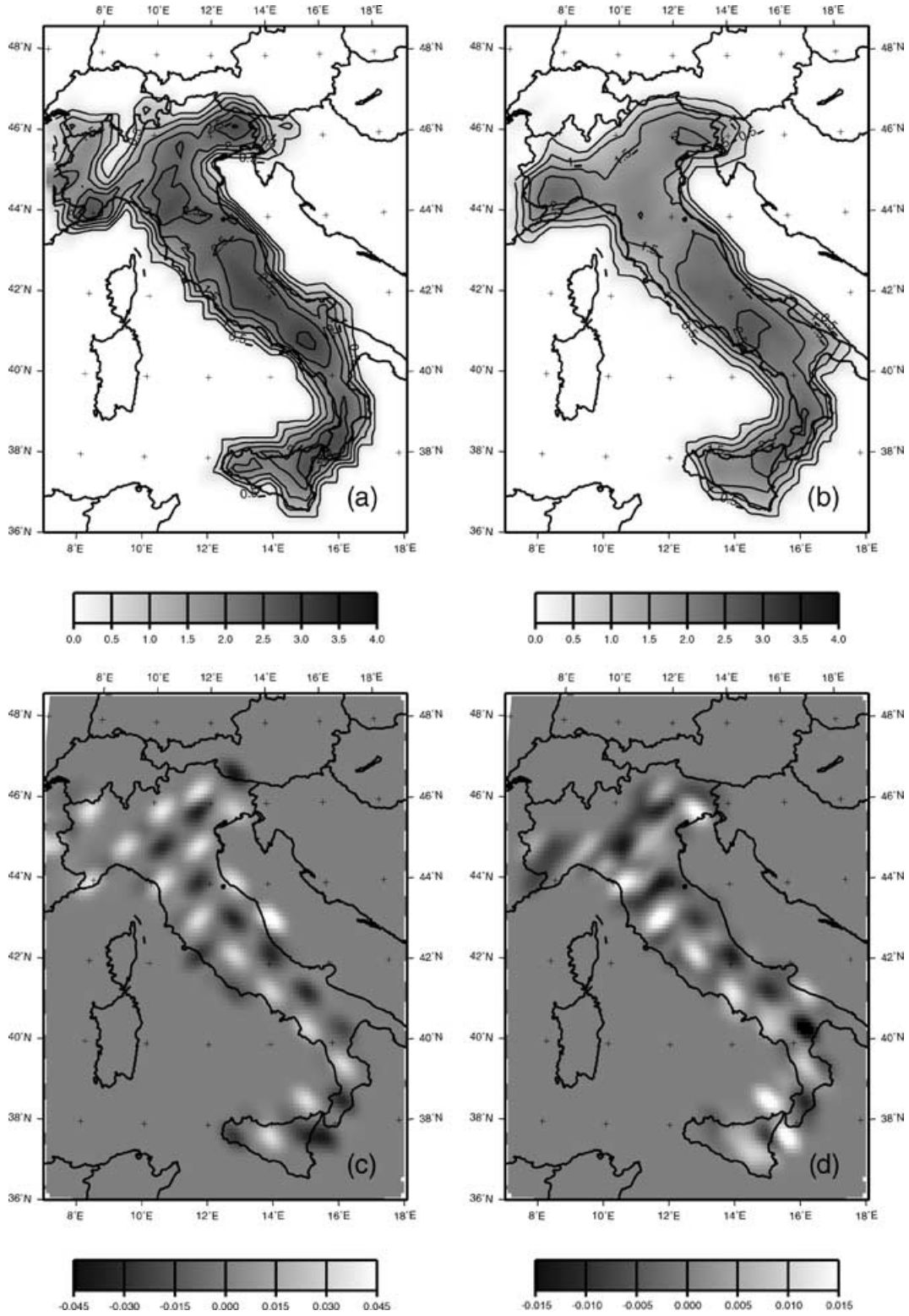

Figure 5. Decimal logarithm of the number of paths contributing to the inversion of coefficient β (a) and γ (b) in each cell. Results of the inversion over a 50 km mesh of a checkerboard imposed harmonic pattern with Gaussian noise added and rounding to nearest half-integer, limited to cells with more than 30 paths for β (c) and γ (d).

Sicily. A narrow and prolonged band with low attenuation follows the outer front of the northern Apennines arc and also extends to the Po valley and the western Alps. We also have low attenuation in eastern Sicily and along the Tyrrhenian coast of the Italian peninsula below latitude 42°, excluding the already mentioned volcanic zones and the area south of the Pollino Massif (between latitude 39° and 40°). The attenuation maxima (located close to active volcanoes) correspond to a decrease of the intensity of about a degree

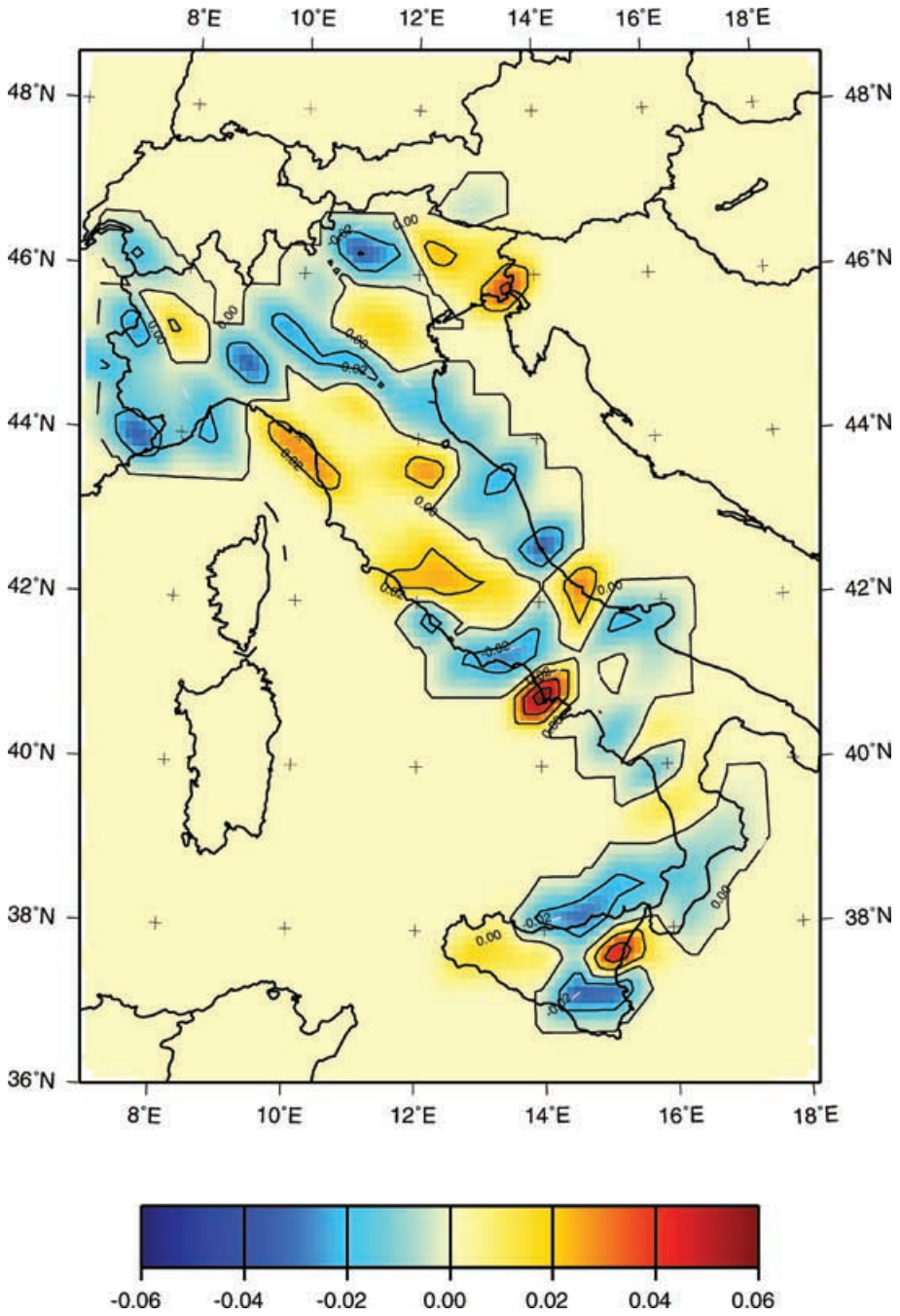

Figure 6. Results of the inversion of real data for attenuation coefficient β ($D < 45$ km) over a 50 km mesh, limited to cells with more than 30 paths.

per 10 km while the minima (in the Po valley, in the Trentino region and in the Eastern Sicily) correspond to about a degree per 50 km.

The spatial variation of the slope γ of the second part of the attenuation curve shows (Fig. 7) a pattern quite different from β. We can note wide areas of low attenuation in the north and a prevalence of high attenuation in the northern and central Apennines. Note the peculiar situation of the northeast of Italy where the far field, showing low attenuation, is in opposition with the near field, showing high attenuation. The areas with highest attenuation are located in the northern Apennines around latitude 44°, in the central Apennines between latitude 41° and 42° and in the south between latitude 38° and 39° close to the Messina strait (between Sicily and Calabria). In the central and southern Apennines we can note an alternation of high- and low-attenuation bands with major elongation in the anti-Apenninic direction and a prevalence of high attenuation along the Tyrrhenian shoreline. The southernmost portion (Calabria and Sicily) shows a prevalence of low attenuation with the only exception of the already mentioned high-attenuation spot located close to the Messina Straits. The attenuation minima correspond to about a degree per 200 km or even more (in northern Italy) while the maxima to a degree per 20 km, comparable to the average values of the near-field coefficient β.

In order to evaluate the role played by the grid spacing we also computed spatial variation of the attenuation coefficients for a finer grid with sides of 25 km. As the number of paths in each cell reduces

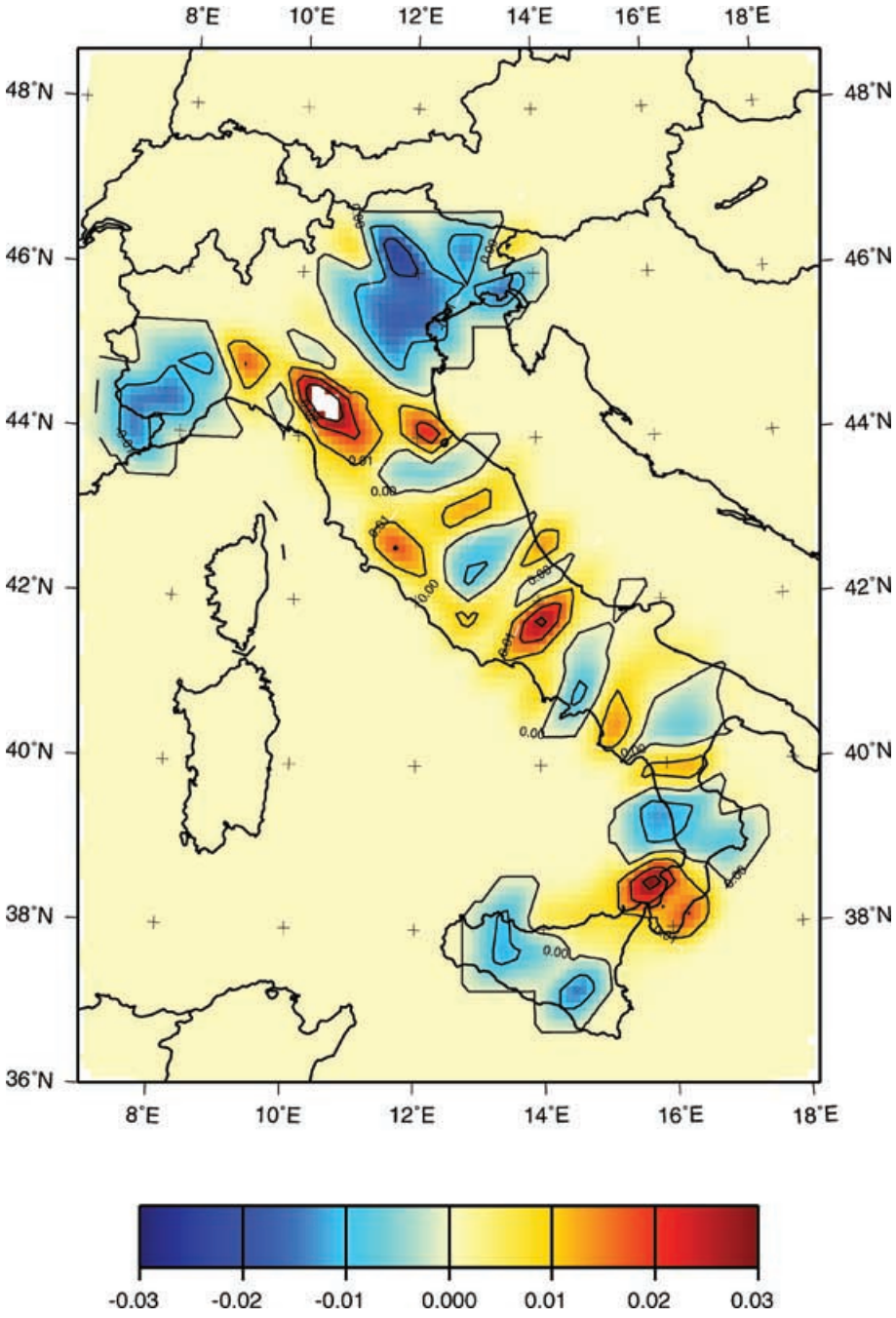

Figure 7. Results of the inversion of real data for attenuation coefficient γ ($D > 45$ km) over a 50 km mesh, limited to cells with more than 30 paths.

on average by a factor of 4, we limited the inversion to the area of central and southern Apennines, shown in Figs 8(a) and (b), best covered by source-to-locality paths (Figs 1, 5a and b). As we still maintain the requirement of having at least 30 crossing paths in a cell, the inverted area is further restricted with respect to previous images. In particular, for β (Fig. 8a), it can be noted how the high-attenuation spot close to Campi Flegrei volcanic area completely disappears due to the low number of paths in the corresponding cells. From the comparison of Fig. 6 with Fig. 8(a) and of Fig. 7 with Fig. 8(b) we can confidently claim that the 25 km inversion confirms the general pattern, albeit with finer detail. In particular, the inversion for γ (Fig. 8b) shows more clearly the sequence of transverse features with alternate properties.

In order to further evaluate the reliability of our results we have also performed a *restore* test, inverting the simulated intensity observations corresponding to the computed variation of attenuation parameters of Figs 6 and 7. As done for the checkerboard test shown above we added a Gaussian noise with a standard deviation of one degree and also rounded the simulated intensities to the nearest half-integer. Figs 9(a) and (b) show that the main features of the imposed patterns are quite well reproduced for both β and γ. The values of misfits are very similar to those computed for the checkerboard test limited to cells with at least 30 paths ($M_\beta = 0.23$, $M_{\gamma\cdot} = 0.40$ and $M_T = 0.32$). In Figs 9(c) and (d) we also reported the plot of the decimal logarithm of standard errors associated with parameter estimates. These lie below -2 (corresponding to about 0.010 deg km^{-1})

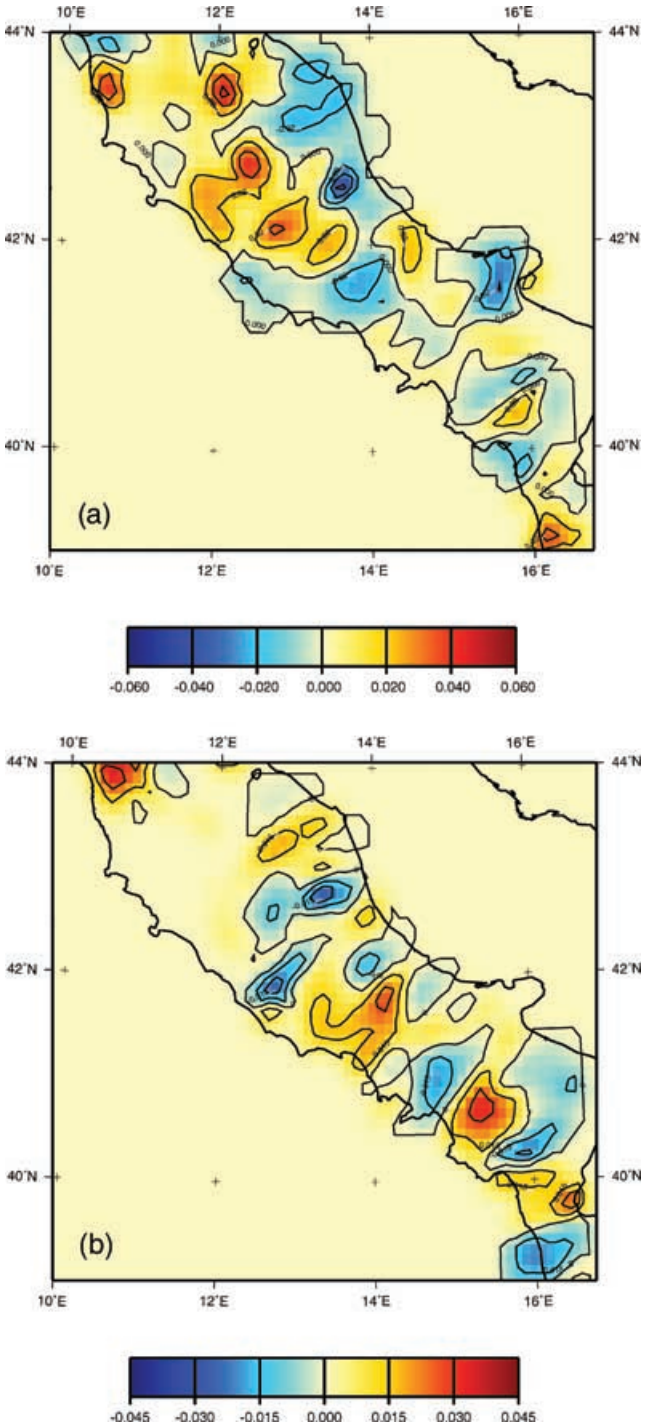

Figure 8. Results of the inversion of real data for attenuation coefficient β (a) and γ (b) over a 25 km mesh, limited to cells with more than 30 paths, for a reduced area of central Italy best covered by hypocentre–locality paths.

on most of the area considered for both parameters. The maximum values are 0.037 deg km^{-1} for β and 0.016 deg km^{-1} for γ but the average values are about 0.005 deg km^{-1} for both parameters. This means that, on average, the errors affect for 10–20 per cent the observed parameters variations (about 0.060 deg km^{-1} for β and 0.045 deg km^{-1} for γ).

Another interesting product of this inversion is the computation of the average site residuals at localities that observed intensities for different earthquakes. These might be correlated with local site soil characteristics and topography and might also help to evaluate the reliability of the data fit, as the existence of trends or regularities in the residuals is a clear symptom of a poor or biased fit. We computed such average deviations at the localities that observed intensity for at least eight different earthquakes. In Figs 10(a) and (b) we reported the negative (red, amplifying), positive (blue, attenuating) and null (black, neutral) site residuals resulting from the application of the isotropic and heterogeneous models, respectively. We can note how for the isotropic model (Fig. 10a) the attenuating sites prevail in the volcanic areas of Tuscany, Latium and around Mt Etna, while amplifying sites dominate along the Adriatic slope of the Apennines. For the heterogeneous model (Fig. 10b), we can observe a general reduction of the residuals and a more uniform distribution of blue and red circles. Amplifying residuals can be observed for centres located along the coasts where the topography effects and liquefaction of soils might justify local amplification. Even the clusters of strongly attenuating sites located in Friuli and around Mt Etna are reduced both in number and in amplitude. This evidence clearly indicates that the heterogeneous model is more effective than the simple isotropic attenuation law in describing the spatial behaviour of the propagation of seismic waves in Italy, thus confirming the reliability of the tomographic inversion.

COMPARISON WITH SEISMIC VELOCITY TOMOGRAPHY STUDIES

Over the last decade, several studies on seismic velocity tomography (SVT) have provided a fairly clear image of the heterogeneities in the crust (Alessandrini *et al.* 1995; Di Stefano *et al.* 1999) and in the mantle (Amato *et al.* 1993, 1998; Spakman *et al.* 1993; Piromallo & Morelli 1997; Mele *et al.* 1998) below the Italian region.

We should not expect a strict correlation between seismic velocity and intensity attenuation variations as the lithological and physical characteristics of the rocks affect the two observables at different depths in a different manner. In fact, in the crust, we could think that seismic velocity is controlled by chemical-compositional variations, while the attenuation should be more influenced by the thermal heterogeneities and by the state of rock fracturing. In the mantle, the thermal heterogeneities should be dominant for both observables, but the effect should be stronger for attenuation. Moreover, most SVT studies only analysed *P* phases while our results are likely to give information mainly on *S*-wave propagation, as shear motion is more effective than the compressional motion at affecting buildings and humans. Nonetheless, as demonstrated by Alessandrini *et al.* (2001) for a small area in central Italy, the pattern of velocity anomalies might be significantly different for *P* and *S* waves.

Among the crustal tomography studies cited above, we must note that the most recent work by Di Stefano *et al.* (1999) can hardly be useful for a comparison as the central reference velocity in each layer (fig. 6 of the cited paper) clearly does not correspond to the average. As the clear imbalance between slow and fast areas testify, the central reference value appears too low for the layer at 8 km depth and too high for the other ones at 22 and 38 km. Moreover, the colour scale clearly saturates at about one-half of the ΔV range, thus preventing a reliable evaluation of the results. Hence, in the following we will only refer to the SVT results by Alessandrini *et al.* (1995), which also have the advantage of being computed with a mesh resolution very similar to that we have used.

In general, we can expect that the temperature variations will produce opposite deviations on attenuation and velocity (a high

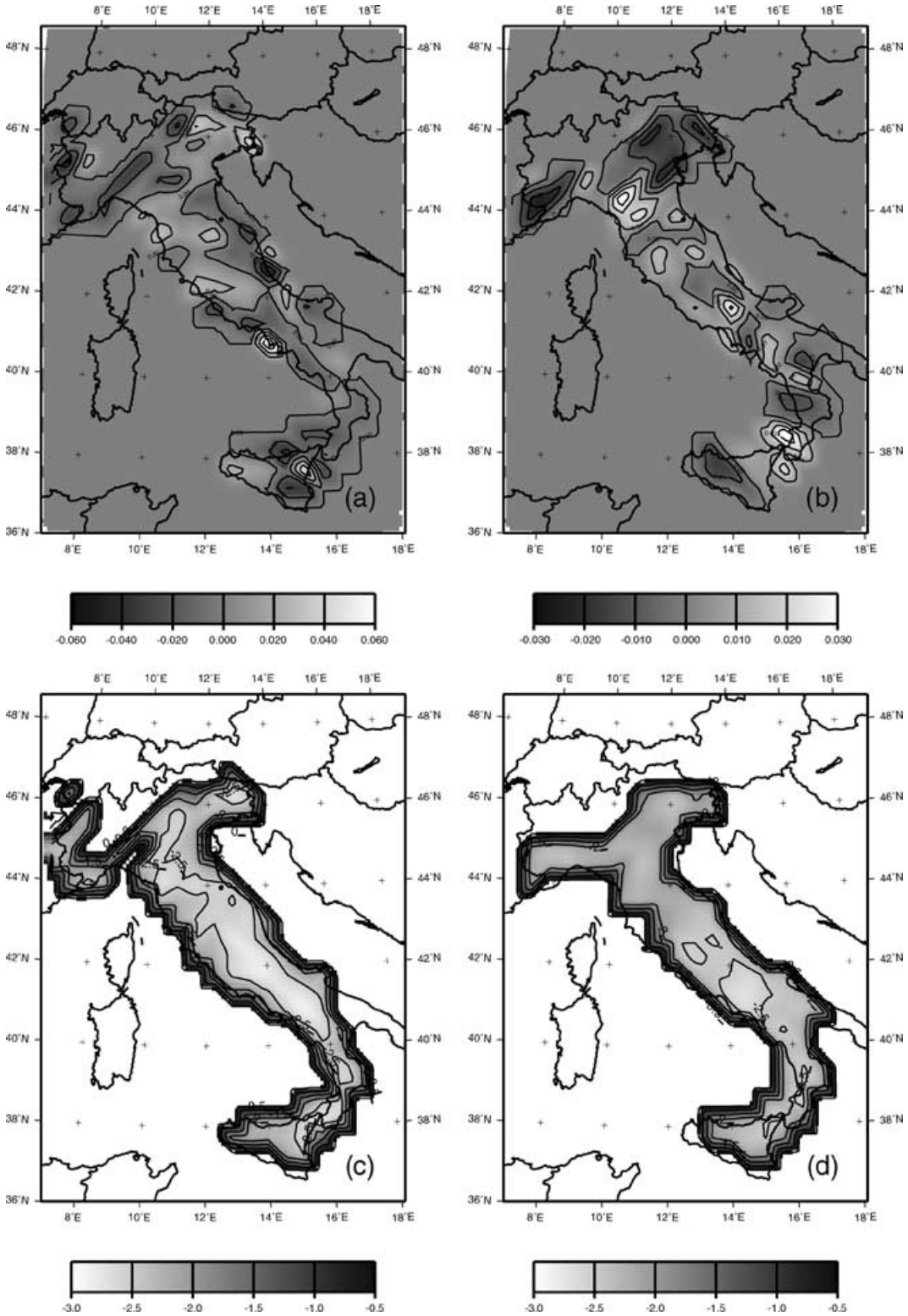

Figure 9. (a), (b) Results of the inversion over a 50 km mesh after the imposition of the inverted pattern (restore test) with Gaussian noise added and rounding to nearest half-integer, limited to cells with more than 30 paths; (c), (d) decimal logarithm of the parameter estimation error, for attenuation coefficient β and γ respectively.

temperature causes high attenuation and low velocity, while a low temperature induces low attenuation and high velocity). These opposite variations, however, are represented in the figures with the same colours, as we indicate high attenuation with red (hot) and low attenuation with blue (cold). Following the geophysical interpretation proposed by Gasperini (2001) we will tentatively consider coefficient β (Fig. 5) as representative of the upper and middle crust and coefficient γ (Fig. 6) of the lower crust and upper portion of the

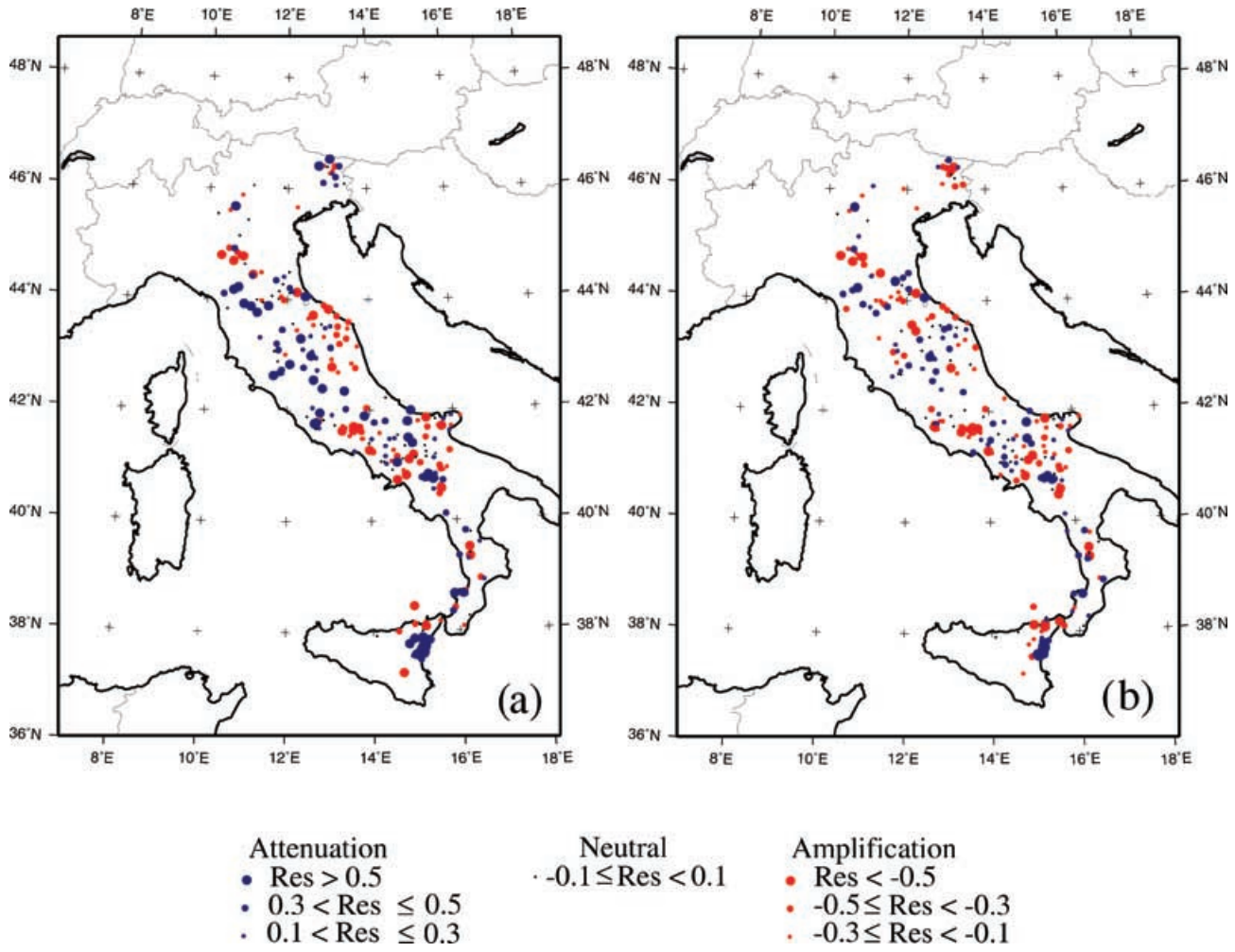

Figure 10. Empirical intensity locality residuals resulting from the application of the isotropic attenuation model (a) and of the tomographic attenuation model (b) for locality having intensity data coming from more than eight different earthquakes.

mantle. So that we will compare the behaviour of the former with figs 15 and 16 of Alessandrini *et al.* (1995), as well as the latter with figs 13 and 14.

For the upper layers we can observe a good coherence between SVT and intensity attenuation in the western Alps but not in the eastern ones. The high attenuation in the easternmost part of northern Italy is, in fact, in opposition to the high velocity deduced by the SVT. Only for the image at 10 km depth can we note a small and weak low-velocity spot in northwestern Italy that disappears at 20 km. For the northern and central Apennines, the high attenuation of the Tyrrhenic slope and the low attenuation in the Adriatic one are confirmed only for the SVT at 10 km but not for the one at 20 km. Even the low-attenuation areas in the Apennines between latitude 41° and 42°, in the southeast of the Italian peninsula and in Eastern Sicily shows a fairly good coherence with the 10 km image but not with the one at 20 km. Although these correspondences could be due just to chance, we can assert that the parameter β agrees fairly well with the velocity variations at 10 km depth.

For the lower layer we have good coherence with the inversion at 37 km depth for most of northern Italy and particularly for the easternmost part, although the intensity attenuation completely misses a red area (high temperature) in the western Alps. In the northern Apennines three strong attenuation highs are only barely counteracted by three weak spots of the SVT that, however, are located almost exactly in the same positions as the former ones. In the central and southern Apennines there is a fairly good correspondence between attenuation heights and velocity lows in Tuscany, Molise, southern Calabria, and between attenuation lows and velocity highs in an area north of the Campi Flegrei and in Central Calabria (Sila massif). The comparison with the solution at 33 km depth shows instead a general disagreement. In particular, in central Apennines the SVT indicates high velocities on the Tyrrhenian slope and low velocities on the Adriatic one that are not reflected by corresponding anomalies in the attenuation. Even in the southern part of the Italian peninsula and in Sicily the disagreement is quite evident. We can conclude that the coefficient γ agrees fairly well with the velocity variations at 37 km depth but not with the ones at 33 km. This best agreement with the deeper SVT image could support the hypothesis formulated by Gasperini (2001) of a subcrustal path for the phases carrying most of the seismic energy at distances longer than 45 km.

COMPARISON WITH INSTRUMENTALLY DERIVED ATTENUATION CURVES

The most comprehensive review of regional variations of the attenuation of ground acceleration in Italy currently available in the literature is the work by Castro *et al.* (1999). They compared the

non-parametric attenuation functions (NAF) previously published for different regions of Italy and also computed average functions for the entire Italian region. The NAF method has the advantage of not requiring a separation of the different effects (anelastic attenuation, geometrical spreading, scattering, source, etc.) and allows an analysis of the attenuation of seismic waves in different regions simply by describing the observed amplitude decay with distance. For each frequency f, the observed acceleration spectral amplitudes $U_i(r, f)$ are modelled as

$$U_i(r, f) = S_i A(r, f), \tag{7}$$

where $A(r, f)$ is obtained by linearizing the previous equation by a logarithmic transformation and inverting for the S_i scalar (one for each earthquake) and discrete values of the attenuation function. $A(r, f)$ is constrained to be a smooth decreasing function of r with a value of unity at a distance of zero (e.g. Anderson & Quaas 1988; Castro *et al.* 1990, 1996).

As a physical relation between seismic intensity and ground motion amplitude does not exist, the comparison with these results might appear quite hard. However, on the basis of a number of empirical studies available in the literature (i.e. Gutenberg & Richter 1956; Trifunac & Brady 1975), a simple linear relation between intensity and the logarithm of ground motion parameters (displacement, velocity, acceleration, etc.) can be tentatively assumed to be, to first order at least,

$$\log_{10}(A) = h + kI, \tag{8}$$

where A is the measured ground motion amplitude, I is the intensity and h and k are empirical coefficients. While h depends on the considered ground motion parameter and on the physical units and hence cannot be unequivocally estimated, k is independent of them and is usually close to 0.3 (Kövesligethy 1906; Gutenberg & Richter 1956; Trifunac & Brady 1975; Panza *et al.* 1997). This means that the ground motion amplitude approximately doubles for an increase of one degree of intensity. Combining eqs (7) and (8) gives

$$\log_{10}(S_i) + \log_{10} A(r, f) = h + kI(r). \tag{9}$$

We can reasonably assume that the source term S_i is a linear function of epicentre acceleration and hence of epicentre intensity

$$\log_{10}(S_i) = g + kI_0 \tag{10}$$

substituting in the previous equation we can obtain

$$\log_{10} A(r, f) = h - g + k[I(r) - I_0]. \tag{11}$$

Hence to compute the NAF using our macroseismic intensity attenuation function we can simply apply the normalization constraint, choosing the value of the parameter g so as to impose $\log_{10} A(0, f) = 0$. Following this approach we have computed the macroseismic equivalent of the NAF for the same areas analysed by Castro *et al.* (1999), on the basis of regional averages of the inverted attenuation coefficients β and γ. Following Castro *et al.* (1999) in Fig. 11(a) we also report the average of the first five regions.

Assuming that the frequencies most likely to induce the largest macroseismic effect (on buildings and humans) are ~2–3 Hz, we can tentatively compare our results with those reported by Castro *et al.* (1999) for instrumental data at 2.5 Hz (Fig. 11b). In general the distance decay of macroseismic intensity appears slightly slower than ground acceleration but the overall range of variations for the average curve is not very different. In agreement with the instrumental results, the less attenuating areas are Eastern Sicily and Lombardia, the most attenuating is central Apennines, while Marche is close to the average. In contrast, the Piemonte–Lombardia and Friuli regions are in disagreement with instrumental data. For Piemonte–Lombardia we do not observe the strong attenuation of the instrumental NAF and the curve almost exactly coincides with that of the Lombardia region alone. On the other hand, the behaviour, shown in the work of Castro *et al.* (1999), of this region is quite peculiar as it strongly attenuates below 10 Hz, while it shows a markedly slow decay for higher frequencies. For the Friuli region, which is close to the Italian average for the instrumental data, we have the strongest attenuation among all regions in the near field and the mildest one in the far field. Although the strong simplifications made and the uncertainties of our inversion process cannot

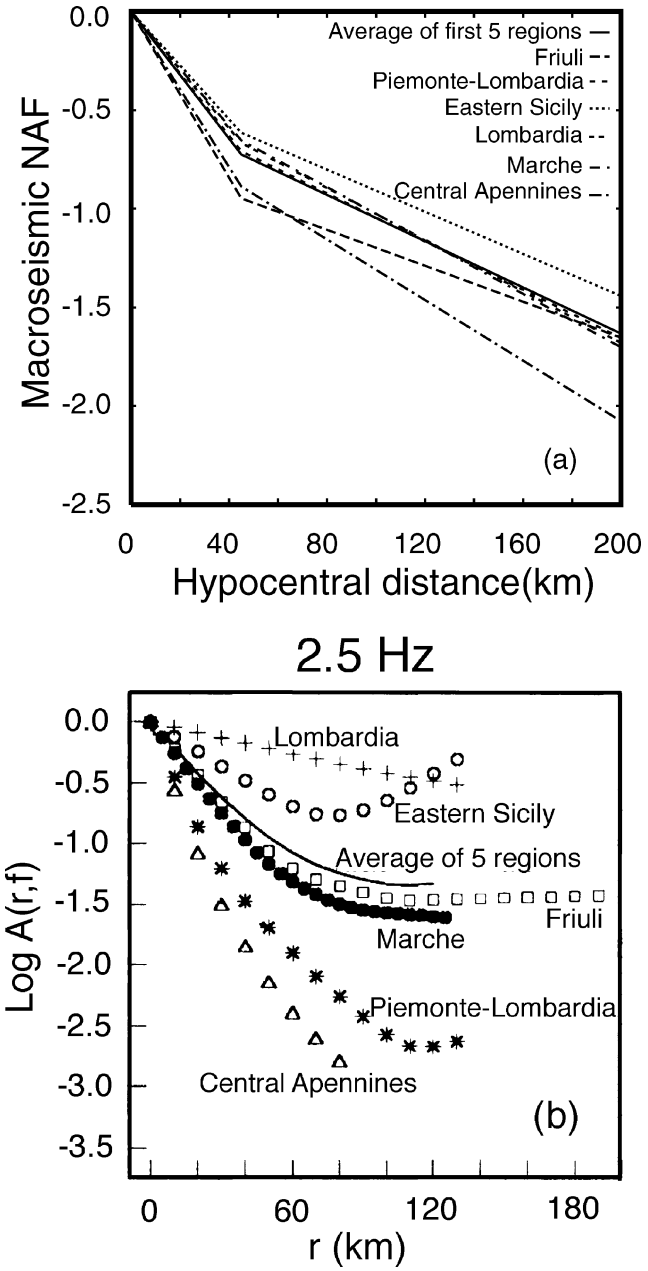

Figure 11. Comparison between the macroseismic equivalent of the non-parametric attenuation function (a) and the instrumentally inferred NAF at 2.5 Hz (b) (modified from Castro *et al.* 1999) for six Italian regions and the average of the first five regions.

allow one to draw definitive conclusions, we can suggest that there is a fairly good coherence between macroseismic and instrumentally determined attenuation functions.

COMPARISON WITH OTHER GEOPHYSICAL OBSERVATIONS

As we have already mentioned the attenuation of seismic waves in rocks depends strongly on temperature, hence, in principle, the spatial variations of attenuation coefficients should be related to such parameters. Although the temperature profile in the crust and upper mantle is not known in detail, we can anyhow consider the surface heat flow as an index of the thermal state in the underlying lithosphere. Assuming constant conductivity and neglecting the effect of radioactive generation, the temperature at depth would be approximately proportional to the surface heat flow. This conductive assumption is not correct in many geothermal areas where a significant fraction of the heat transport is due to the circulation of fluids. However, to first order at least, a direct correspondence between high heat flow values and high temperatures at depth can be confidently assumed.

For the Italian area, while the Ligurian and Tyrrhenian seas are relatively well covered by heat flow measurements, the data in the mainland and in the Adriatic and Ionian Basins are rather sporadic and concentrated in very few areas (see Pollack *et al.* 1993). Hence the reliability of the large-scale features of the heat flow map of Italy (Della Vedova *et al.* 1991; Cataldi *et al.* 1995) suffers from this irregular data distribution and thus must be considered with care when comparing such a map with other geophysical observations.

Nonetheless the similarity between the inversion results for parameter β (Fig. 5) and the map by Della Vedova *et al.* (1991) (Fig. 12) is rather clear. In particular, the well-known geothermal area along the Tyrrhenian coast of Tuscany and Latium (with heat flow values up to some hundreds of mW m^{-2}) clearly corresponds to the extended positive (high-attenuation) anomaly of our results. Moreover, such a correspondence can also be found between the high heat flow spots located close to volcanic areas (Campi Flegrei and Mt Etna) and localized positive anomalies of the attenuation. Furthermore, the dominance of low heat flow values in Sicily and southern Italy below latitude 41° (excluding volcanic areas) agrees well with a diffuse prevalence of low attenuation in the same areas. It is also interesting to note the good match between a prolonged band with relatively high heat flow ($q_s > 50$–60 mW m^{-2} with two spots with $q_s > 80$ mW m^{-2}) extending southeastward, from the Adriatic coast around latitude 42°, along the eastern slope of the southern Apennines with a similar spatial pattern of the attenuation coefficient β, best demonstrated in the detailed image of Fig. 8(a). In reasonable agreement with this physical interpretation, is the relatively high heat flow observed in northeastern Italy, in correspondence with the magmatic intrusion of the Colli Euganei and Monti Lessini as well as of the spot (with $q_s > 70$ mW m^{-2}), along the Adriatic coast between Venice and Trieste which might justify, at least in part, the high attenuation of northeastern Italy. A mismatch can be noted only in northwestern Italy where, however, our inversion is less reliable due to reduced path density (see Fig. 1).

The results of the inversion for the coefficient γ, which we assumed to refer to deeper features are instead less clearly correlated with the heat flow. Although the prevalence of high attenuation in the northern Apennines and along the Tyrrhenian shoreline are still coherent with heat flow data, some other features such as the extended low-attenuation area in the northeast and the high-attenuation spot in Calabria would probably require a more complex explanation involving the variations of the crust thickness and the presence of a subducted slab below the southern Tyrrhenian Sea.

The crustal thickness itself is another kind of spatial data that is usually compared with seismic tomography results (see e.g. Alessandrini *et al.* 1995). During the last few decades several authors have approached the problem of determining the Moho depth in Italy both from inversion of gravity anomalies (Giese & Morelli 1975; Baldi *et al.* 1982) and from deep seismic soundings (Nicolich 1981; Ambrosetti *et al.* 1987; Nicolich & Dal Piaz 1990). These maps are not immediately comparable with our colour-shaded images as they are plotted with contour lines. Moreover, those derived from seismic soundings show many apparent discontinuities due to the lack of data. Referring to the most recent paper by Nicolich & Dal Piaz (1990) (also reproduced by Alessandrini *et al.* 1995) we can note for both β and γ a prevalence of low attenuation in areas characterized by crust thicker than 35 km (Alps, northern Apennines, Tyrrhenian slope of the southern Apennines, Calabria, Tyrrhenian coast of Sicily). For γ this could be interpreted as being due to the lower attenuation of the colder sinking crust of the roots of mountain chains with respect to the surrounding hotter upper mantle, while for β this could be related to the relatively higher heat flow coming from the mantle in areas where the crust is thinner.

Even the Bouguer gravity anomalies can be directly compared with tomographic images. The most prominent features of the map compiled by Carrozzo *et al.* (1990) for the Italian region (even in this case reproduced by Alessandrini *et al.* 1995) are the prevalence of negative anomalies along the Adriatic slope of the Apenninic Chain and in central Sicily with some isolated positive anomalies in the Western Alps ('Corpo di Ivrea') in the Paleogene volcanic area of Colli Euganei and Monti Lessini and in the northern Adriatic Sea. Positive anomalies prevail instead in the Tyrrhenian Sea and surrounding mainland areas, and in the southern Adriatic Sea including the Apulian Plain. Negative anomalies usually indicate an excess of crustal material lighter than the reference density used for the Bouguer correction or a thicker layer of light rocks. In general, we can observe for β a general dominance of low attenuation in areas with negative anomalies and of high attenuation in areas with positive anomalies, while for γ the situation is almost reversed although no strict correlations among the fine features of the different maps can be found.

DISCUSSION AND CONCLUSIONS

Although the nature of different physical processes (geometrical spreading, anelastic dissipation and seismic scattering) responsible for the attenuation of seismic waves is well known, their balance and thus their contribution to the observed amplitude decrement with distance is a rather complex and still unresolved problem. Moreover, the uncertainties for source and site responses also contribute to make this matter more complex with relevant consequences on the reliability of PSHA. In the current literature, the practical solution adopted is the fit of empirical attenuation functions that, neglecting some or all of the details of single physical processes, allow one to make predictions of the expected ground shaking amplitude at the site. Among them we can mention the NAF method described above, the simple regressions between distance and the logarithm of PGA (Campbell 1985; Sabetta & Pugliese 1987, 1996) or even spectral approaches that make use of simplifying assumptions to separate the different terms (e.g. Malagnini *et al.* 2000).

The main limitation of these techniques in predicting the levels of ground motion in PSHA is the strong variability of attenuation

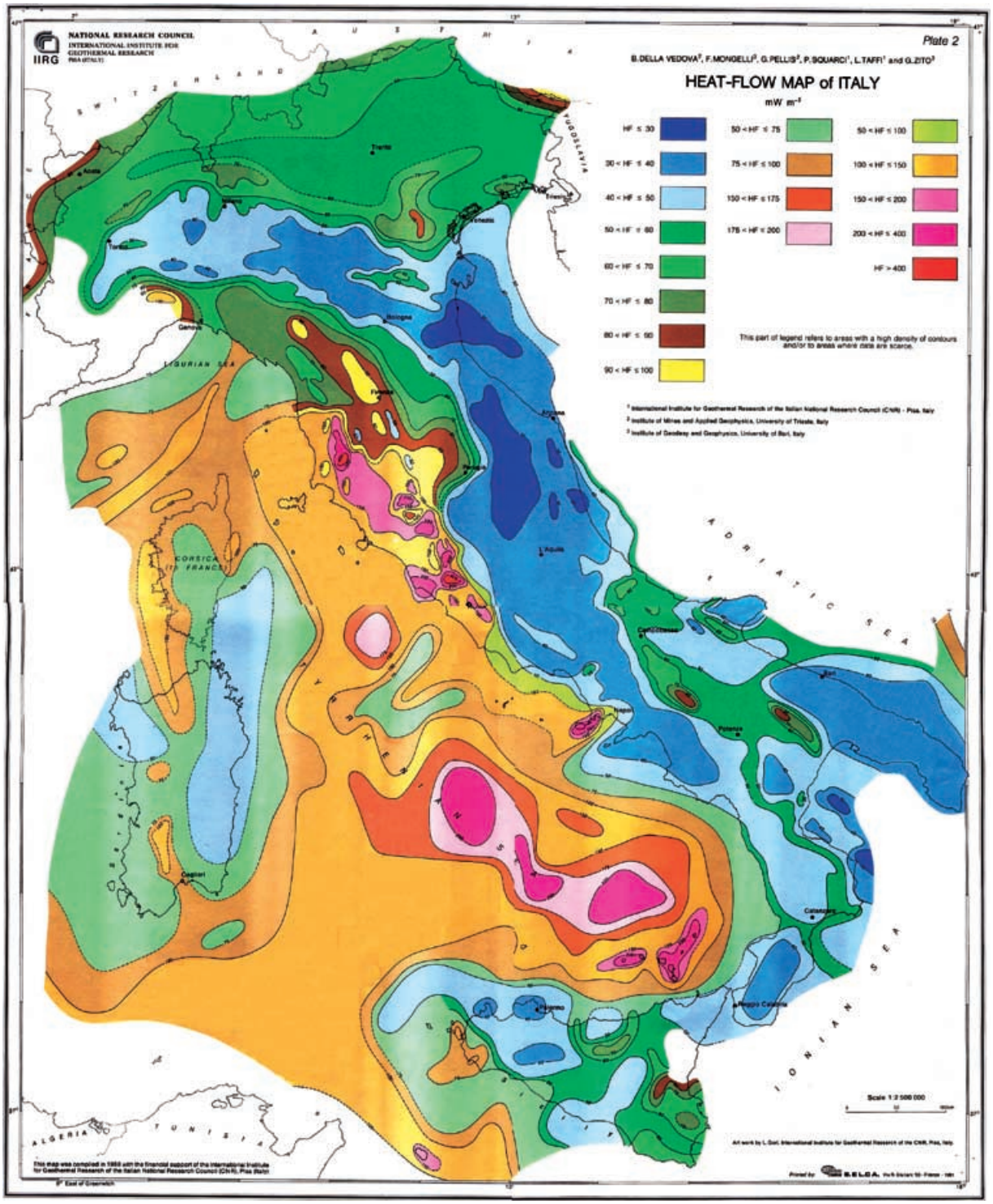

Figure 12. Heat flow map of Italy (after Della Vedova *et al.* 1991; Cataldi *et al.* 1995).

properties from one region to another. This variability, which is reflected by a strong scatter of the data for attenuation relations derived for the whole territory, also prevents the extrapolation of regionalized relations to different areas of the country. Within this framework, our tomographic inversion could be useful for calibrating the instrumentally derived attenuation function in order to extend their applicability for areas not yet investigated. Our approach, in fact, although referring to non-instrumental quantities, is able to map the lateral variation of seismic attenuation in most of the Italian territory. Its reliability was confirmed by the results of checkerboard and restore tests, which indicate that the macroseismic data set is able to constrain the lateral variations of attenuation coefficients with a spatial resolution of 50 km. Moreover, both the marked reduction of locality residuals and their more uniform distribution with respect to an isotropic model, demonstrate that the lateral variations of attenuation coefficients give a meaningful description of the properties of

seismic wave propagation in the Italian area. Nevertheless, the clear correlation found between the spatial variations of the near-field ($D < 45$ km) coefficient with the map of the heat flow in Italy supports the existence of a physical grounding for our approach.

As we have shown that a macroseismic equivalent of the NAF, in fair agreement with instrumentally derived ones, can be deduced from our results, it should be possible to develop a methodology to calibrate, using the macroseismic inversion results, the regional NAFs or the spectral scaling relations, deduced by instrumental data analysis, for widespread usage over the whole country.

A more straightforward application of our results is the prediction of the levels of ground motion at a site in terms of macroseismic intensity. We have found, however, that the variance reduction of the heterogeneous tomographic model with respect to the isotropic bilinear one is only about 14 per cent. Although this is not bad if compared, for example, with the values of about 20–30 per cent typical of instrumental SVT inversions (i.e. Di Stefano *et al.* 1999), we must admit that the improvement in ground motion predictions achieved by the inclusion of propagation heterogeneities is not very significant. Part of this scattering is certainly due to the uncertainties related to the macroseismic intensity assignment process that, as is well known, is rather subjective and, for the MCS intensity, almost completely neglects the robustness and the state of preservation (the vulnerability) of the involved buildings.

However, it is also well known that local soil characteristics and topography at the evaluated sites may contribute to amplification or attenuation of the level of ground motion. Soft soils and sharp topographies are usually associated with amplification as well as solid rock basements and mild topographies inducing an attenuation of ground motion and hence of the damaging effects on buildings and goods. The site empirical residuals resulting after our inversion, being deprived of the propagation term, should be representative of the site effects only and thus could give a chance to further improve our ability to predict the macroseismic intensity. For a future work we plan a systematic comparison of intensity average residuals with the geological and topographical characteristics of sites in order to evaluate whenever they are actually correlated with local site conditions or are instead purely random deviations due to the uncertainties of the process. If such a correlation is found, we could assume our empirical residuals to be representative of the local site condition and use them to further reduce the uncertainties of hazard estimates.

Another point that could be considered in the near future, both to improve the resolution of the mapping of attenuation coefficients, as well as the ability to predict the ground motion levels in the near field, is the computation of more realistic source-locality distances considering the spatial extension and the orientation of seismic sources. In fact, although the focal plane solutions of most of the earthquakes included in our database is not known, we could make use of the technique developed by Gasperini *et al.* (1999) to infer the orientation and the spatial extension of the sources directly from macroseismic data. Another possibility to be explored is to invert the source orientations, minimizing the solution residuals, simultaneously to the tomographic problem. Both of these methods would allow one to compute more precise source to locality distances to be used in PSHA and also to further reduce the uncertainties of the tomographic inversion.

ACKNOWLEDGMENTS

We want to thank the macroseismic researchers of *Storia Geofisica Ambiente* (SGA) and of *Gruppo Nazionale Difesa dai Terremoti* (GNDT), whose continuous effort over the last two decades made available to the scientific community the very high quality data we have used. We also thank Andrea Morelli, Claudia Piromallo and Giuliana Mele for valuable suggestion on tomographic techniques. The comments of an anonymous referee helped to clarify the limits and the physical meaning of our results. This work was carried out within the ambit of the Framework Programme 2000/2002 of GNDT. It has also been supported by the *Istituto Nazionale di Geofisica e Vulcanologia* (INGV), which funded the PHD grant of one of the authors (FC), and by the Italian Ministry of Education, University and Research (MIUR). Most figures were drawn by the Generic Mapping Tool (GMT) (Wessel & Smith, 1991).

REFERENCES

Alessandrini, B., Beranzoli, L. & Mele, F.M., 1995. 3-D crustal *P*-wave velocity tomography of the Italian region using local and regional seismicity data, *Ann. Geofis.,* **38,** 189–211.

Alessandrini, B., Filippi, L. & Borgia, A., 2001. Upper crust tomographic structure of the Central Apennines, Italy, from local earthquakes, *Tectonophysics,* **339,** 479–494.

Amato, A., Alessandrini, B. & Cimini, G., 1993. Teleseismic-wave tomography of Italy, in *Seismic Tomography: Theory and Practice,* pp. 361–396, eds Iyer, H.M. & Hirahara, K., Chapman and Hall, London.

Amato, A. *et al.,* 1998. Passive seismology and deep structure in Central Italy, *Pure appl. Geophys.,* **151,** 479–493.

Ambrosetti, P., Bosi, C., Carraro, F., Ciaranfi, M., Panizza, N., Papani, G., Vezzani, L. & Zanferrari, A., 1987. *Neotectonic Map of Italy: scale 1:500,000,* Progetto Finalizzato Geodinamica, CNR.

Anderson, J.G. & Quaas, R., 1988. The Mexico earthquake of September 19, 1985: effect of magnitude on the character of strong ground motion: an example from the Guerrero, Mexico strong motion network, *Earthquake Spectra,* **4,** 635–646.

Baldi, P., Degli Angioli, E., Piallini, L. & Mantovani, E., 1982. Gravity anomaly interpretation in the Calabrian Arc and surrounding regions: three-dimensional approach, *Earth Evol. Sci.,* **3,** 243–247.

Berardi, R., Petrungara, C., Zonetti, L., Magri, L. & Mucciarelli, M., 1993. *Mappe di Sismicità per l'Area Italiana,* ISMES, Bergamo (Italy), p. 52.

Boschi, E., Guidoboni, E., Ferrari, G., Valensise, G. & Gasperini, P., 1997. *Catalogo dei Forti Terremoti in Italia dal 461 a.C. al 1990,* ING/SGA Bologna (Italy), p. 644, also available at http://storing.ingrm.it.

Campbell, K.W., 1985. Strong-motion attenuation of peak horizontal acceleration, *Earthquake Spectra,* **1,** 759–804.

Carrozzo, M.T., Luzio, D., Margiotta, C. & Quarta, T., 1990. Gravity map of Italy, in *Structural Model of Italy and Gravity Map,* eds Bigi, G., Cosentino, D., Parotto, M., Sartori, R. & Scandone, P., CNR, S.E.L.C.A., Firenze.

Castro, R.R., Anderson, J.H. & Singh, S.K., 1990. Site responce, attenuation and source spectra of *S* waves along the Guerrero, Mexico, subduction zone, *Bull. seism. Soc. Am.,* **80,** 1481–1503.

Castro, R.R., Pacor, F., Sala, A. & Petrungaro, C., 1996. *S* wave attenuation and site effects in the region of Friuli, Italy, *J. geophys. Res.,* **101,** 22 355–22 369.

Castro, R.R., Mucciarelli, M., Monachesi, G., Pacor, F. & Bernardi, R., 1999. A review of nonparametric attenuation functions computed for different regions of Italy, *Ann. Geofis.,* **42,** 735–748.

Cataldi, C., Mongelli, F., Squarci, P., Taffi, L., Zito, G. & Calore, C., 1995. Geothermal ranking of Italian territory, Geothermics, **24,** 115–129.

CPTI Working Group, 1999. *Catalogo Parametrico dei terremoti Italiani,* p. 88, Editrice. Compositori, Bologna, Italy, also available at http://emidius.itim.mi.cnr.it/CPTI/home.html.

Della Vedova, B., Mongelli, F., Pellis, G., Squarci, P., Taffi, L. & Zito, G., 1991. *Heat flow map of Italy,* International Institute for Geothermal Research, CNR-Pisa.

Di Stefano, R., Chiarabba, C., Lucente, F. & Amato, A., 1999. Crustal and uppermost mantle structure in Italy from the inversion of *P*-wave arrival times: geodynamic implications, *Geophys. J. Int.,* **139,** 483–498.

Fäh, D. & Panza, G., 1994. Realistic modelling of observed seismic motion in complex sedimentary basin, *Ann. Geofis.,* **37,** 1771–1797.

Fletcher, J.B. & Boatwright, J., 1991. Source parameters of Loma Prieta aftershocks and wave propagation characteristics along the San Francisco peninsula from a joint inversion of digital seismograms, *Bull. seism. Soc. Am.,* **81,** 1783–1812.

Gasperini, P., 2001. The attenuation of seismic intensity in Italy: a bilinear shape indicates the dominance of deep phases at epicentre distances longer than 45 km, *Bull. seism. Soc. Am.,* **91,** 826–841.

Gasperini, P. & Ferrari, G., 2000. Deriving numerical estimates from descriptive information: the computation of earthquake parameters, *Ann. Geofis.,* **43,** 729–746.

Gasperini, P., Bernardini, F., Valensise, G. & Boschi, E., 1999. Defining seismogenic sources from historical earthquake felt reports, *Bull. seism. Soc. Am.,* **89,** 94–110.

Giese, P. & Morelli, C., 1975. Crustal structure in Italy, in *Structural Model of Italy, Quaderni della Ricerca Scientifica,* **90,** 453–489.

Gutenberg, B. & Richter, C.F., 1956. Earthquake magnitude, intensity, energy and acceleration, *Bull. seism. Soc. Am.,* **46,** 105–145.

Gupta, I.N. & Nuttli, O.W., 1976. Spatial attenuation of intensities for central US earthquakes, *Bull. seism. Soc. Am.,* **66,** 743–751.

Hashida, T. & Shimazaki, K., 1984. Determination of seismic attenuation structure and source strength by inversion of seismic intensity data: method and numerical experiment, *J. Phys. Earth,* **32,** 299–316.

Hashida, T., Stavrakakis, G. & Shimazaki, K., 1988. Three-dimensional seismic attenuation structure beneath the Aegena region and its tectonic implication, *Tectonophysics,* **145,** 43–54.

Kövesligethy, R., 1906. A makroszeimikus rengések feldogozása, *Math. és Termé, szettudamányi Értesitõ,* **24,** 349–368.

McGarr, A., Çelebi, M., Sembera, E., Noce, T. & Mueller, C., 1991. Ground motion at the San Francisco international airport from the Loma Prieta earthquake sequence, 1989, *Bull. seism. Soc. Am.,* **81,** 1923–1944.

Malagnini, L., Herrmann, R.B. & Di Bona, M., 2000. Ground-motion scaling in the Apennines (Italy), *Bull. seism. Soc. Am.,* **90,** 1062–1081.

Mele, G., Rovelli, A., Seber, D. & Barazangi, M., 1996. Lateral variation of P_n propagation in Italy: evidence for a high-attenuation zone beneath the Apennines, *Geophys. Res. Lett.,* **23,** 709–712.

Mele, G., Rovelli, A., Seber, D., Hearn, T.H. & Barazangi, M., 1998. Compressional velocity structure and anisotropy in the uppermost mantle beneath Italy and surrounding regions, *J. geophys. Res.,* **103,** 12 529–12 543.

Monachesi, G. & Stucchi, M., 1997. DOM4.1, un database di osservazioni macrosismiche di terremoti di area italiana al di sopra della soglia del danno, GNDT, *Open File Report,* Milano-Macerata, also available at http://emidius.itim.mi.cnr.it/DOM/home.html.

Nicolich, R., 1981. Crustal structures of the Italian peninsula and surrounding areas: a review of DSS data, in *Sedimentary Basins of Mediterranean Margins,* pp. 3–17, ed. Wezel, F.C., CNR, Tecnoprint, Bologna.

Nicolich, R. & Dal Piaz, R., 1990. Moho isobaths, in *Structural Model of Italy and Gravity Map,* **Sheet 2,** eds Bigi, G., Cosentino, D., Parotto, M., Sartori, R. & Scandone, P., CNR.

Panza, G.F., Cazzaro, R. & Vaccari, F., 1997. Correlation between macroseismic intensities ans seismic ground motion parameters, *Ann. Geofis.,* **40,** 1371–1382.

Papazachos, C., 1992. Anisotropic radiation modelling of macroseismic intensities for estimation of the attenuation structure of the upper crust in Greece, *Pageophys.,* **138,** 445–469.

Papazachos, C. & Papaioannou, C., 1997. The macroseismic field of the Balkan area, *J. Seism.,* **1,** 181–201.

Piromallo, C. & Morelli, A., 1997. Imaging the Mediterranean upper mantle by *P*-wave travel time tomography, *Ann. Geofis.,* **40,** 963–979.

Pollack, H.N., Hurter, S.J. & Johnson, J.R., 1993. Heat flow from the earth's interior: analysis of the global data set, *Rev. Geophys.,* **31,** 267–280.

Romeo, R. & Pugliese, A., 1997. La pericolosità sismica in Italia. Parte 1: analisi della scuotibilità. National Seismic Service Report SSN/RT/97/1, Rome, Italy.

Sabetta, F. & Pugliese, A., 1987. Attenuation of peak horizontal acceleration and velocity from Italian ground-motion records, *Bull. seism. Soc. Am.,* **77,** 1491–1511.

Sabetta, F. & Pugliese, A., 1996. Estimation of response spectra and simulation of nonstationary earthquake ground motion, *Bull. seism. Soc. Am.,* **86,** 337–352.

Sieberg, A., 1932. Erdebeben, in *Handbuch der Geophysik,* Vol. 4, pp. 552–554, ed. Gutenberg, B., Gebrueder Borntraeger Verlag, Berlin.

Slejko, D., 1996. Preliminary seismic hazard assessment for the Italian seismic code, in *Earthquake Hazard and Risk,* pp. 87–124, ed. Schenk, V., Kluwer, Dordrecht.

Somerville, P. & Yoshimura, J., 1990. The influence of critical Moho reflections on strong ground motion recorded in San Francisco and Oakland during the 1989 Loma Prieta earthquake, *Geophys. Res. Lett.,* **17,** 1203–1206.

Spakman, W., van der Lee, S. & van der Hilst, R., 1993. Travel-time tomography of the European–Mediterranean mantle down to 1400 km, *Phys. Earth planet. Inter.,* **79,** 3–74.

Trifunac, M.D. & Brady, A.G., 1975. On the correlation of seismic intensity scales with peaks of recorded strong ground motion, *Bull. seism. Soc. Am.,* **65,** 139–162.

Wells, D.L. & Coppersmith, K.J., 1994. New empirical relationships among magnitude, rupture length, rupture width, rupture area and surface displacement, *Bull. seism. Soc. Am.,* **84,** 974–1002.

Wessel, P. & Smith, W.H.F., 1991. Free software helps map and display data, *EOS Trans., AGU.,* **72,** 441–461.